Rotary Empirical Orthogonal Function Analysis of Currents near the Oregon Coast

D. W. DENBO AND J. S. ALLEN

School of Oceanography, Oregon State University, Corvallis, OR 97331

(Manuscript received 24 May 1983, in final form 18 August 1983)

ABSTRACT

Empirical orthogonal function (EOF) analysis in the frequency domain is extended to complex time series. EOFs are calculated from the eigenvectors of the band-averaged rotary cross-spectral matrix. This gives EOF amplitude and phase for negative and positive frequencies, corresponding to clockwise and anticlockwise rotation for the hodograph model. Rotary EOF analysis is applied to velocity and temperature measurements from the Coastal Upwelling Experiment (CUE-II) during July and August 1973 on the continental shelf off Oregon. Rotary EOFs for horizontal velocities are computed for the diurnal, near-inertial and semidiurnal frequency bands (approximately 1.0, 1.5 and 2.0 cycles per day, respectively) and for frequency bands below 0.3 cycles per day. In addition, single-sided frequency-space EOFs for vertical displacement are calculated from temperature measurements. The first-mode velocity EOF for the semidiurnal frequency band shows baroclinic structure for clockwise rotation and barotropic structure for anticlockwise rotation. This separation of vertical structure by the direction of rotation is consistent with a barotropic tide forcing a baroclinic response. The first-mode displacement EOF amplitude functions are coherent with first-mode velocity–amplitude functions at the semidiurnal frequency for both rotations, with a 180° phase difference between displacement and surface velocity indicating an onshore propagating internal wave. In the near-inertial frequency band, the first-mode velocity EOF phase for clockwise rotation has a linear slope above 60 m corresponding to an upward phase propagation at 0.14 cm s^{-1} and downward energy propagation. This is in agreement with results of Kundu (1976) obtained from the same observations in a different manner. For the diurnal frequency band, the first-mode velocity EOFs are depth independent below 15 m for both rotations. From 15 m upward, the rotary velocity EOF for clockwise rotation increases rapidly in amplitude. The surface intensification is associated with a 180° phase change near 15 m. The clockwise and anticlockwise velocity EOF–amplitude functions at the diurnal frequency are coherent with the wind stress and with each other. This coherence with wind stress and the surface intensification indicates a wind-forced surface layer. The vertical structure and coherences are consistent with near-zero depth-integrated mass transport normal to the coast, where the wind-forced surface transport is compensated by a transport in the opposite direction below.

1. Introduction

Empirical orthogonal function (EOF) analysis in the frequency domain was developed for applications in meteorological data analysis by Wallace and Dickinson (1972). It has been applied to oceanographic problems by Wang and Mooers (1977), Hogg (1981) and Halliwell and Mooers (1983). Frequency-domain EOF analysis involves computing a band-averaged cross-spectral matrix for several real time series and then calculating the eigenvectors and eigenvalues of that matrix. The complex eigenvectors are used to compute the EOF amplitude and phase.

Rotary spectral analysis is discussed in detail by Gonella (1972) and Mooers (1973). It involves writing a horizontal velocity-vector time series as a complex one, where the real and imaginary parts are orthogonal velocity components. The Fourier transform of the complex time series then gives Fourier coefficients for positive and negative frequency. Rotary spectra may be interpreted in terms of the hodograph model for two-dimensional velocity vectors (Mooers, 1973). In the hodograph model, the autospectra for positive and negative frequencies are interpreted as resulting from two independent vectors rotating anticlockwise and clockwise, respectively. When these vectors are added together, the resultant vector rotates clockwise or anticlockwise and traces an ellipse whose characteristics are described by Gonella (1972).

In this paper we combine frequency-domain EOF analysis and rotary spectral analysis to calculate rotary empirical orthogonal functions. The rotary EOF analysis is formally similar to single-sided frequency-domain EOF analysis. The primary difference is that the time series are complex, rather than real, and the frequency is two-sided, i.e., positive and negative. The extension of single-sided frequency-domain EOF analysis with real functions to rotary, two-sided frequency-domain EOF analysis with complex functions is analogous to the extension of time-domain EOF analysis from real to complex time series described by Kundu and Allen (1976).

The method presented here is applied to velocity and temperature measurements from the Coastal Upwelling Experiment (CUE-II) which took place during the summer of 1973 on the continental shelf off Oregon. The investigation concentrates primarily on the semidiurnal, near-inertial and diurnal frequency bands and on low frequencies of less than 0.3 cycles per day (cpd).

2. Data

The data utilized are a subset of the observations made as part of the Coastal Upwelling Experiment (CUE-II) conducted during the summer of 1973 near 45°16'N on the continental shelf off Oregon. The observations span nearly two months and include velocity and temperature measurements from five moorings (Fig. 1). The moorings Forsythia, Edelweiss, Carnation, and Aster were deployed by Oregon State University. The data are described by Kundu and Allen (1976). Buoy-B was deployed by the Pacific Marine Environmental Laboratory, and the data are described by Halpern (1976a). The measurements, originally taken at 10–15 min intervals, were filtered with a low-pass filter having a half-power point of 12 cycles per day (cpd) and then subsampled to hourly values.

The data are divided into two sets for the purposes of the following analyses. The first is a "vertical" data set which includes 11 horizontal current and 9 temperature measurements from the Buoy-B and Carnation moorings (Table 1). The two moorings were in 100 m of water and were less than 2 km apart. Since the coherence squared between the Buoy-B measurements at 18 m and the Carnation measurements at 20 m, for the frequency bands used here, are typically greater than 0.7, these two sets of measurements are treated as if they are from a single mooring. A common

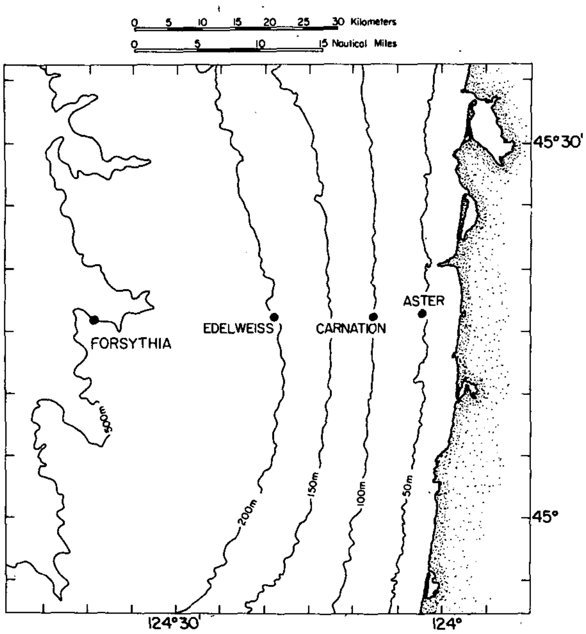

FIG. 1. Bottom topography and location of the CUE-II current meter moorings used here. Moorings Buoy-B and Carnation were less than 2 km apart.

TABLE 1. Vertical data set.

Mooring	Instrument	Depth (m)	Bottom depth (m)	Location	Weight B_j
Buoy-B	B3	3	100	45°15.8'N	0.056
	B8	8		124°07.8'W	0.032
	B10	10			0.033
	B14	14			0.032
	B16	16			0.020
	B18	18			0.020
Carnation	C20	20	100	45°16.2'N	0.111
	C40	40		124°06.9'W	0.202
	C60	61			0.202
	C80	81			0.177
	C95	96			0.117

time period of 54 days beginning 5 July 1973 is used for the analyses. The second set is composed of "cross-shelf" data which include current measurements at 16 positions from the Forsythia, Edelweiss, Carnation and Aster moorings (Table 2). A common time period of 32 days beginning 25 July 1973 is used for the analyses.

The wind measurements are from the surface mooring at Buoy-B. Hourly wind stress was computed from the hourly wind velocity, extrapolated to the 10 m level with a logarithmic wind profile, using an aerodynamic square law with a constant drag coefficient of 1.3×10^{-3} (Halpern, 1976b).

3. Rotary empirical orthogonal functions

We consider a set of N discrete complex time series

$$w_j(t_m) = u_j(t_m) + iv_j(t_m), \quad m = 1, \ldots, M, \quad (3.1)$$

where u_j and v_j are real time series of orthogonal velocity components at position $j(j = 1, \ldots, N)$,

TABLE 2. Cross-shelf data set.

Mooring	Instrument	Depth (m)	Bottom depth (m)	Location	Weight B_j
Forsythia	F40	44	500	45°16.8'N	0.142
	F80	88		124°39.6'W	0.095
	F120	127			0.119
	F180	188			0.142
Edelweiss	E20	19	200	45°16.2'N	0.096
	E80	81		124°18.7'W	0.096
	E120	121			0.096
	E180	181			0.063
	E195	196			0.022
Carnation	C20	20	100	45°16.2'N	0.032
	C40	40		124°06.9'W	0.021
	C60	61			0.021
	C80	81			0.017
	C95	96			0.012
Aster	A20	21	50	45°16.4'N	0.019
	A40	43		124°01.5'W	0.008

$t_m = m\Delta t$ is the discrete time, Δt the sampling interval, M the even number of data points in the series and $i = (-1)^{1/2}$. The Fourier coefficients for $w_j(t_m)$ are

$$W_j(f_n) = \left(\frac{1}{M}\right)\sum_{m=1}^{M} w_j(t_m)\exp(-2i\pi t_m f_n), \quad (3.2)$$

$$n = -\frac{M}{2}, \ldots, \frac{M}{2} - 1,$$

where $f_n = n/(M\Delta t)$ is the discrete frequency. Positive and negative frequencies correspond to two-dimensional, horizontal velocity vectors rotating in anticlockwise and clockwise directions at frequency $|f_n|$, respectively.

The rotary empirical orthogonal functions (EOFs) are the eigenvectors e_j^i determined by solving the eigenvalue problem

$$\sum_{j=1}^{N} C_{kj}e_j^i = \lambda^i e_k^i, \quad k = 1, \ldots, N \quad (3.3)$$

where e_j^i is the ith ($i = 1 \cdots N$) eigenvector with corresponding eigenvalue λ^i,

$$C_{kj} = \overline{W_k^* W_j}(B_k B_j)^{1/2}$$
$$= \sum_{m=n-\Delta n}^{n+\Delta n} W_k^*(f_m)W_j(f_m)(B_k B_j)^{1/2}, \quad (3.4)$$

is the weighted, band-averaged, rotary cross-spectral matrix centered at frequency f_n with bandwidth $(2\Delta n + 1)/(M\Delta t)$, Δn is a positive integer,

$$\overline{(\ )} = \sum_{m=n-\Delta n}^{n+\Delta n} (\ ), \quad (3.5)$$

is the band-averaging operator, and an asterisk denotes complex conjugate. The B_j are real weighting functions and may be used to normalize C_{kj} or to scale variables with different magnitudes. They are left unspecified at this time. Since C_{kj} is a Hermitian matrix, the eigenvalues are real and the eigenvectors are orthogonal. We normalize the eigenvectors so that

$$\sum_{k=1}^{N} e_k^{i*}e_k^j = \delta_{ij}, \quad (3.6)$$

where δ_{ij} is the Kronecker delta function. Each eigenvector e_j^i may be multiplied by an arbitrary complex number g^i, where $g^{i*}g^i = 1$. We choose g^i such that e_1^i is real.

The Fourier coefficients may be expanded in terms of the eigenvectors e_j^i such that

$$W_j(f_m) = \sum_{k=1}^{N} e_j^{k*}Z^k(f_m)B_j^{-1/2},$$

$$m = n - \Delta n, \ldots, n + \Delta n. \quad (3.7)$$

The $Z^k(f_m)$ are the rotary-EOF amplitude functions and are obtained by multiplying (3.7) by e_j^i and summing over j:

$$Z^i(f_m) = \sum_{j=1}^{N} e_j^i W_j(f_m)B_j^{1/2},$$

$$m = n - \Delta n, \ldots, n + \Delta n. \quad (3.8)$$

The EOF amplitude functions of frequency f_m have a domain of $f_n \pm \Delta n/(M\Delta t)$, i.e., they are defined for the frequencies over which the rotary cross-spectral matrix is band-averaged.

The band-averaged cross-spectra for the rotary EOF amplitude functions are

$$\overline{Z^{i*}Z^j} = \sum_{k,n=1}^{N} e_k^{i*}C_{kn}e_n^i = \lambda^i\delta_{ij}. \quad (3.9)$$

The rotary-EOF amplitude functions are incoherent over the frequency band $f_n \pm \Delta n/(M\Delta t)$ and have band-averaged autospectra λ^i.

We point out that frequency-domain EOFs and time-domain EOFs are formally similar, where frequency and time are the respective independent variables. The band-averaged cross-spectral matrix is analogous to the covariance matrix. The cross-spectra between any other complex time series and the EOF amplitude function may be computed directly using $Z^i(f_m)$, where the frequency band used for the cross-spectral calculations is the domain of the amplitude function.

The dimensional amplitude and the phase of the EOF are given by

$$A_j^i = |e_j^i|(\lambda^i/B_j)^{1/2}, \quad (3.10)$$

$$P_j^i = \tan^{-1}[-\mathrm{Im}(e_j^i)/\mathrm{Re}(e_j^i)], \quad (3.11)$$

respectively, for mode i and position j. Since e_1^i is real, the EOF phase P_j^i is relative to position $j = 1$, i.e., $P_1^i = 0$. The percent of the variance of the series at position j explained by mode i is given by

$$V_j^i = (A_j^{i2}/\overline{W_j^* W_j}) \times 100. \quad (3.12)$$

The percent of the variance explained (V_j^i) and the EOF phase (P_j^i) may also be determined by computing the coherence squared and phase from the cross-spectra of the mode i amplitude function with series j. Utilizing (3.7) and (3.9), we obtain

$$\overline{Z^{i*}W_j} = \lambda^i e_j^{i*}B_j^{-1/2}. \quad (3.13)$$

The coherence squared and phase from (3.13) are

$$\mathrm{coh}_j^{i2} = |\overline{Z^{i*}W_j}|^2/(\overline{Z^{i*}Z^i}\,\overline{W_j^* W_j})$$
$$= e_j^{i*}e_j^i\lambda^i B_j^{-1}/(\overline{W_j^* W_j})$$
$$= A_j^{i2}/\overline{W_j^* W_j} = V_j^i/100, \quad (3.14)$$

$$\Phi_j^i = \tan^{-1}[\mathrm{Im}(\overline{Z^{i*}W_j})/\mathrm{Re}(\overline{Z^{i*}W_j})]$$

$$= \tan^{-1}[-\mathrm{Im}(e_j^i)/\mathrm{Re}(e_j^i)] = P_j^i, \qquad (3.15)$$

respectively. Thus, as with single-sided frequency-domain EOFs (Wallace and Dickinson, 1972) the coherence squared between the EOF amplitude function and series j can be interpreted as the fraction of the variance of that series explained by the EOF. Also, we see that the phase from the cross-spectra between the EOF amplitude function and series j is the same as the EOF phase.

The trace of the cross-spectral matrix is

$$\sum_{k=1}^{N} C_{kk} = \sum_{i=1}^{N} \lambda^i = \sum_{k=1}^{N} \overline{W_k^* W_k} B_k. \qquad (3.16)$$

Thus, if the weighting functions B_k are not 1, the trace of C_{kj} is not equal to $\sum_{k=1}^{N} \overline{W_k^* W_k}$, the sum of the band-averaged autospectra of $w_k(t_m)$. Since C_{kj} depends on B_k, the total variance explaned by mode i, λ^i, depends on the weighting.

Rotary autospectral statistics (Gonella, 1972) may be applied to the EOF amplitude functions. The rotary coefficient

$$C_r^i(f_n) = (S_+^i - S_-^i)/(S_+^i + S_-^i), \qquad (3.17)$$

where

$$S_\pm^i = \overline{Z^{i*}(\pm|f_n|)Z^i(\pm|f_n|)} \qquad (3.18)$$

gives the partition of the total variance for mode i between the EOF amplitude functions for clockwise and anticlockwise rotation. The outer autospectra

$$R^i = \overline{Z^i(+|f_n|)Z^i(-|f_n|)} \qquad (3.19)$$

is used to compute the ellipse stability squared

$$|E^i|^2(f_n) = |R^i|^2/(S_-^i S_+^i) \qquad (3.20)$$

and ellipse orientation

$$\Phi_r^i(f_n) = \tfrac{1}{2}\tan^{-1}[\mathrm{Im}(R^i)/\mathrm{Re}(R^i)], \qquad (3.21)$$

measured anticlockwise from east (Mooers, 1973).

We note that the formulas presented in this section are also valid for single-sided EOF analysis if a single-sided Fourier trnsform is used in place of (3.2). One utility of the method described here is that it allows the direct computation of the cross-spectra between an EOF amplitude function and any other complex series. The same method applies, of course, for single-sided EOFs. This makes the construction of the augmented time series, introduced by Wallace and Dickinson (1972), unnecessary in either case.

4. Analysis

Rotary spectra for wind stress measured at Buoy-B and for currents measured at B8 are plotted in Fig. 2.

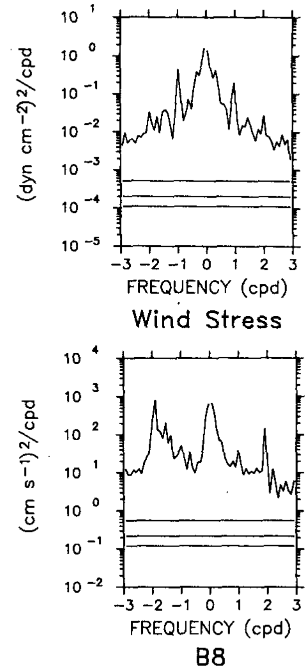

FIG. 2. Rotary spectra of wind stress measured at Buoy-B (top) and of currents measured at B8 (bottom). The band width is 0.093 cpd. Note the spectral peaks for B8 at the semidiurnal (±1.91 cpd), near-inertial (−1.54 cpd) and diurnal (±0.98 cpd) frequencies and for wind stress at the diurnal (±0.98 cpd) frequency. The 90% confidence levels are indicated by horizontal lines.

For the wind stress, there are significant peaks in the spectra at the diurnal frequency (±0.98 cpd). For the currents at B8, there are significant peaks in the spectra at the near-inertial (−1.54 cpd), semidiurnal (±1.91 cpd) and diurnal (±0.98 cpd) frequencies. These peaks are present in most current spectra and motivate a concentration of our analysis on these frequency bands. The frequency at which the near-inertial spectral peak occurs (−1.54 cpd) is 1.08 times the local inertial frequency, in agreement with the results of Kundu (1976) from the same data. There are ten degrees of freedom per frequency band in the spectral calculations and in the following EOF analysis, corresponding to bandwidths of 0.093 and 0.16 cpd for the vertical and cross-shelf data sets, respectively. The rotary spectra and cross-spectra for this data are described in greater detail by Denbo (1983).

Empirical orthogonal function calculations for the semidiurnal, near-inertial, diurnal and low frequency bands were made using the velocity and temperature observations in the vertical data set. Rotary velocity EOFs were computed where u_j and v_j in (3.1) are, respectively, the eastward and northward velocity components at location j. Time series of vertical displacement ζ were computed from the temperature time series and the vertical gradient of time averaged temperature $d\bar{T}/dz$ (Fig. 3) where $\zeta = T/(d\bar{T}/dz)$. Single-sided EOFs for displacement were calculated using the

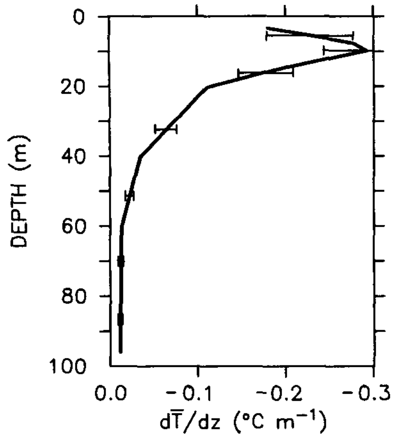

FIG. 3. The mean vertical temperature gradient $d\bar{T}/dz$ (°C m^{-1}) as a function of depth (m) calculated from the mean temperature measured at the Buoy-B and Carnation moorings. The standard error for $d\bar{T}/dz$ is denoted by horizontal lines.

rotary formalism (3.1) with $u_j = \zeta_j$ and $v_j = 0$. The rotary spectra for displacement are symmetric about zero frequency. Similarly, rotary EOFs for displacement at $\pm|f_n|$ have amplitudes that are equal and phases with the opposite sign. A benefit of using the rotary formalism with displacement is that the cross-spectral calculations between the displacement-EOF amplitude function and rotary spectral coefficients are facilitated.

Rotary velocity EOFs are also calculated for the semidiurnal, diurnal and low-frequency bands using the cross-shelf data set. EOFs were not computed for the near-inertial frequency band since in that band coherence between currents measured at different across-shelf locations was generally not significant.

In calculating the cross-spectral matrix $\mathbf{C}_{ij}$, the individual time series are weighted in order to minimize the effects of large differences in nearest instrument separations, which for the vertical data set, for example, range from 2 to 20 m. Since the total energy for dynamical modes is calculated using space integrals, the weighting is based on the spatial separation of the measurements. For the vertical data set, the weight B_j for a given measurement location is given by half the distance to the instrument above plus half the distance to the instrument below divided by the total water depth. For the cross-shelf data set, the weight B_j is given by half the distance to the instrument above plus half the distance to the instrument below times half the distance to the onshore instrument plus half the distance to the offshore instrument divided by the total cross-shelf area represented by the measurements. The individual series from location j are multiplied by $B_j^{1/2}$. The position of each instrument and the corresponding weight are given in Table 1 and Table 2 for the vertical and cross-shelf data sets, respectively. EOFs were computed for both the weighted and unweighted cross-spectral matrices. The differences in the EOFs were typically less than 10% for amplitude and 5% for phase. The results presented in the following sections are from the weighted matrices.

The selection of EOFs significantly different from those produced from white noise is based on a conservative extrapolation from Table 1 of Overland and Preisendorfer (1982). An EOF mode is assumed to be significant if at least 50% of the total variance is explained by mode 1 or 40% by mode 2. Only significant EOF modes, which here are limited to mode 1, are discussed.

5. Semidiurnal frequency band

a. *Vertical EOFs*

The amplitudes and phases for the first rotary velocity EOFs calculated from the vertical data set are plotted in Fig. 4 as functions of depth for the semidiurnal frequency band centered at $|f| = 1.91$ cpd. The EOFs (or modes) are denoted as 1_- and 1_+ for clockwise and anticlockwise rotation, respectively. The 1_- EOF, with 85% of the total clockwise variance, has a baroclinic structure with a zero crossing near 30 m. The amplitude function is not significantly coherent with the rotary wind stress measured at Buoy-B (Table 3). Phase is nearly constant above and below 30 m with a rapid change of 180° near 30 m. The anticlockwise 1_+ EOF amplitude is nearly depth-independent and is smaller than that of the clockwise 1_- EOF. The phase is also nearly depth-independent, so that the mode 1_+ structure is similar to that of a barotropic tide. The 1_+ EOF contains 90% of the total anticlockwise variance and its amplitude function is not significantly coherent with the wind stress.

Rotary statistics calculated for the 1_+ and 1_- velocity-EOF amplitude functions are presented in Table 3.

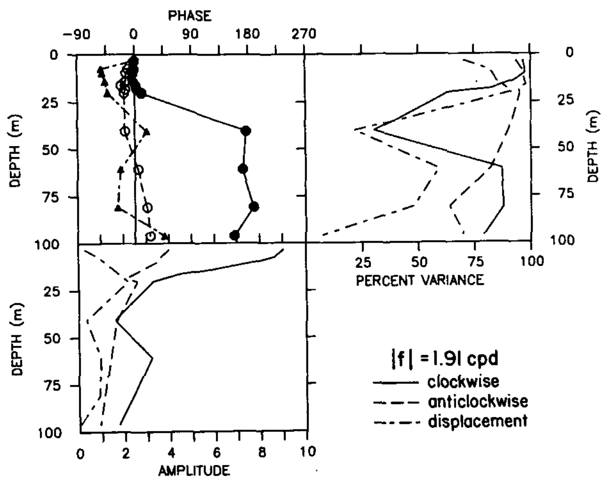

FIG. 4. Rotary first-mode velocity- and displacement-EOF phase (top), amplitude (bottom) and percent variance explained (upper right) as functions of depth (m) for the semidiurnal frequency band (1.91 cpd) and the vertical data set. The velocity- and displacement-EOF amplitudes are in cm s^{-1} and m, respectively. Phase for the displacement EOF has been shifted by 180° for display purposes.

TABLE 3. Percent of the total variance explained by the first rotary velocity EOF, rotary EOF statistics, and cross-spectra of the rotary velocity-EOF amplitude function versus wind stress for vertical data set.

Frequency (cpd)	Percent variance	C_r	Axis orientation (deg)	$\|E\|^2$	EOF vs wind stress Coh^2	Phase (deg)	EOF leads (days)
−1.91	85	−0.59	2	0.62	0.49	−34	0.05
−1.54	64	−0.90	56	0.02	0.16	−44	0.08
−0.98	90	−0.51	13	0.67	0.90	59	−0.17
−0.24	80	0.00	24	0.33	0.72	64	−0.74
−0.15	96	0.00	81	0.71	0.48	−5	0.08
−0.06	89	−0.17	−29	0.26	0.66	172	−8.58
0.06	84				0.58	67	3.33
0.15	90				0.23	32	0.59
0.24	83				0.73	67	0.77
0.98	82				0.66	113	0.32
1.54	58				0.02	60	0.11
1.91	90				0.47	−48	−0.07

The rotary coefficient is negative, indicating a clockwise rotating vector. The ellipse is oriented across shelf and has high stability squared reflecting high coherence between these modes.

The displacement EOF has a nearly constant phase with depth and a maximum amplitude at 20 m (Fig. 4). The coherences between the displacement- and velocity-EOF amplitude functions are significant and are summarized in Table 4. The coherence between the displacement-EOF amplitude function and the rotary wind stress is not significant for either clockwise or anticlockwise rotations (Table 5). The baroclinic structure of mode 1_- and the location of the maximum in displacement-EOF amplitude near the depth of the clockwise velocity-EOF node are consistent with a semidiurnal first vertical-mode internal wave. The phase between the velocity- and displacement-amplitude functions, together with the EOF phase for velocity and displacement (Fig. 4), imply that for a positive displacement there is offshore flow above 30 m and onshore flow below 30 m, i.e., there are 180° and 0° phase differences between velocity and displacement above and below 30 m, respectively. This phase relation between the velocity and displacement indicates onshore propagation of the internal wave as was found on the continental shelf off Northwest Africa by Gordon (1978).

The EOF amplitudes and phases for mode 1_- and 1_+, consequently, appear to represent an M_2 barotropic tide forcing an M_2 baroclinic tide which rotates primarily clockwise and propagates onshore. This interpretation also finds some support in theoretical arguments. Gonella (1972) has shown, from the following approximate form of the momentum equations, $\partial w/\partial t + if_0 w = \gamma$, where $w = u + iv$, γ is a periodic forcing function with equal clockwise and anticlockwise components, and f_0 the Coriolis parameter, that the response w at the semidiurnal frequency will be primarily clockwise with a theoretical rotary coefficient of −0.95. Müller *et al.* (1978) found the same theoretical rotary coefficient for a random ensemble of free internal waves at the semidiurnal frequency. Also, Torgrimson and Hickey (1979) have argued, based on the slope of internal wave characteristics, that the generation of the semidiurnal internal tide in this region is most likely to occur at depths in the ranges 200 to 500 m and 500 to 1000 m. As a result, the baroclinic tide on the shelf in 100 m water depth may be expected to rotate clockwise and may be larger in amplitude than the barotropic tide, in agreement with the EOF results.

b. Cross-shelf EOFs

The 1_- EOF amplitude and phase calculated from the cross-shelf data set are presented using polar coordinates in Fig. 5. The base of the vectors indicates the location of the instrument, the length of the vector represents the amplitude, and the anticlockwise angle from the vertical represents positive phase. The phases are relative to F40. Mode 1_-, with 79% of the total clockwise variance, has phase changes in the vertical through approximately 180° near F180, E80 and C40, and the EOF amplitude is a minimum at these locations. These features, together with the horizontal differences in EOF phase and the propagation direction inferred from the EOFs of the vertical data set, indicate an internal wave with a node in the vertical at approximately 0.4 times the local water depth (F180, E80 and C40) propagating onshore with a cross-shelf wavelength of 40 km. The contours in Fig. 5 of variance explained by mode 1_- for the complex time series show that a small percentage of the variance from instruments near the nodes is explained by mode 1_-. This supports the interpretation of a baroclinic mode since the time series at F180, E80 and C40 are not unusually low in variance for this frequency band.

The 1_+ EOF is nearly depth-independent (Fig. 5). Mode 1_+ with 90% of the total anticlockwise variance has an amplitude approximately half the mode 1_- amplitude. All the time series, except that from F80, have a high percentage of their anticlockwise variance explained by mode 1_+. The predominant pattern is nearly

TABLE 4. Coherence squared and phase for first displacement EOF versus first rotary velocity EOF for the vertical data set.

Frequency (cpd)	Clockwise (−) velocity EOF [Coh^2/Phase (deg)]	Anticlockwise (+) velocity EOF [Coh^2/Phase (deg)]
1.91	0.88 30	0.74 −37
1.54	0.28 140	0.04 −13
0.98	0.88 117	0.67 −142

TABLE 5. Percent of the total variance explained by the first displacement EOF and cross-spectra of the displacement-EOF amplitude function versus wind stress for the vertical data set.

		EOF vs clockwise wind stress			EOF vs anticlockwise wind stress		
Frequency (cpd)	Percent variance	Coh^2	Phase (deg)	EOF leads (days)	Coh^2	Phase (deg)	EOF leads (days)
1.91	70	0.33	−64	0.09	0.15	−34	−0.05
1.54	63	0.66	167	−0.30	0.62	46	0.08
0.98	57	0.89	−57	0.16	0.88	−107	−0.30

depth independent with a small amount of shear present. The cross-shelf EOF phase differences, onshore leading, are in the same sense as those caused by bottom friction in the barotropic tidal model of Battisti and Clarke (1982).

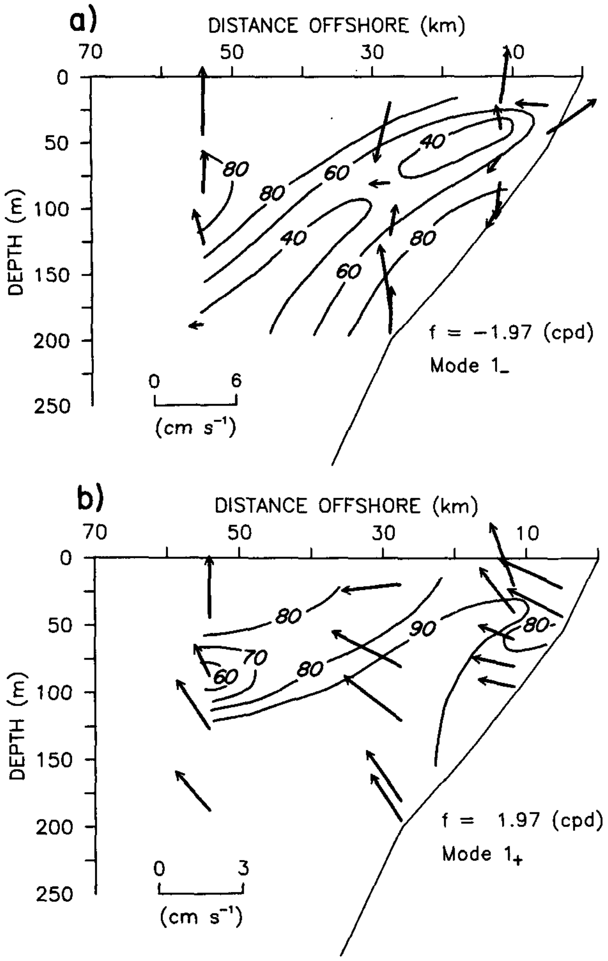

FIG. 5. Rotary first-mode velocity EOF for clockwise (a) and anticlockwise (b) rotation at the semidiurnal frequency (1.97 cpd) for the cross-shelf data set. The EOF amplitude and phase are presented using polar coordinates. The base of the vector indicates the instrument location, the vector length indicates the amplitude (cm s^{-1}) and the angle anticlockwise from the vertical indicates positive phase relative to F40. The percent of the variance of the series at position j explained by this mode is contoured as a function of depth and distance offshore. The contour intervals are 20% and 10% for clockwise and anticlockwise rotation, respectively. The bottom topography is indicated by a solid line of variable depth to the right. Note difference in velocity scale for (a) and (b).

The rotary statistics for the 1_- and 1_+ EOF amplitude functions (Table 6) indicate a clockwise rotating vector with the ellipse oriented across-shelf. The ellipse stability is significant, indicating that the modes 1_- and mode 1_+ are coherent. The cross-shelf EOF amplitude functions are not coherent with the wind stress.

The separation into baroclinic and barotropic structures by rotation found in these cross-shelf EOFs is the same as found from the vertical data set and again is consistent with an M_2 barotropic tide forcing an M_2 baroclinic tide, where the baroclinic response is primarily of clockwise rotation and propagates onshore.

6. Near-inertial frequency band

Vertical EOFs. The velocity-EOF amplitudes and phases calculated from the vertical data set for the near-inertial frequency band centered at $|f| = 1.54$ cpd are plotted as functions of depth in Fig. 6. There is a greater amount of variance explained by the clockwise EOF than by the anticlockwise EOF, which is consistent with the presence of waves of near-inertial frequency and with the peak in the rotary autospectra for clockwise rotation at −1.54 cpd. The mode 1_- amplitude is a maximum at the surface. The mode 1_- EOF phase has a linear slope above 60 m which corresponds to an upward propagation of phase at a velocity of 0.14 cm s^{-1}. This result is efficiently obtained by the rotary spectral EOFs and is in good agreement with the upward propagation of phase at 0.20 cm s^{-1}

TABLE 6. Percent of the total variance explained by the first rotary velocity EOF, rotary EOF statistics, and cross-spectra of the rotary velocity-EOF amplitude function versus wind stress for the cross-shelf data set.

					EOF vs wind stress		
Frequency (cpd)	Percent variance	C_r	Axis orientation (deg)	$\lvert E\rvert^2$	Coh^2	Phase (deg)	EOF leads (days)
−1.97	79	−0.41	6	0.78	0.04	−101	0.14
−1.03	57	0.26	69	0.51	0.84	−102	0.27
−0.25	79	−0.27	−77	0.77	0.39	−136	1.51
0.25	64				0.25	107	1.19
1.03	84				0.78	155	0.42
1.97	90				0.25	16	0.02

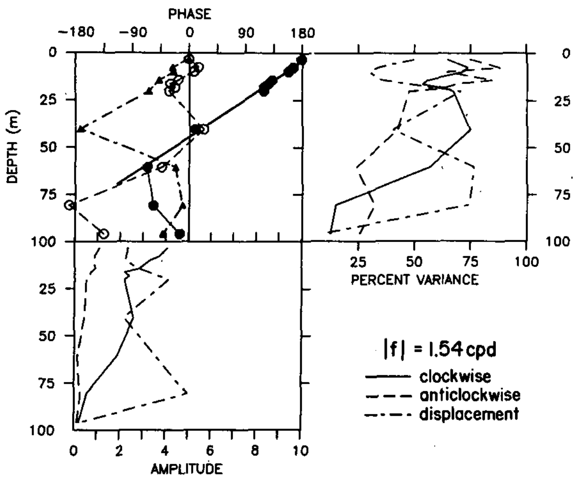

FIG. 6. As in Fig. 4 but for the near-inertial frequency band (1.54 cpd) and the vertical data set. The velocity and displacement EOF amplitudes are in cm s^{-1} and 10^{-1} m, respectively. Phase for the displacement and clockwise-velocity EOF has been shifted by 180° for display purposes.

found by Kundu (1976) from lagged cross-correlations of band-pass filtered cross-shelf velocity components using the same data.

The rotary statistics for the EOF amplitude functions (Table 3), $C_r = -0.9$ and $|E|^2 = 0.02$, confirm the relatively larger clockwise energy and low coherence between the two rotational components. Neither component is significantly coherent with the wind stress, in agreement with previous findings (Gonella, 1972; Davis *et al.*, 1981). This low coherence is evidently caused by the fact that sudden changes in wind stress generate and cancel near-inertial waves in a manner dependent on the relative phase between the wind stress and the existing free waves (Pollard, 1970). It also is possibly due to the response of currents to near-inertial frequency wind stress being governed in part by horizontal variations in the mean flow (Weller, 1982). The low coherence at the near-inertial frequency between velocities at different cross-shelf locations may be due to the latter process.

The mode-one displacement EOF for the near-inertial frequency band (Fig. 6) has a phase structure above 40 m similar to the mode 1_- velocity EOF. This similarity in phase may be fortuitous, however, since only one displacement-EOF phase value above 40 m is significant because of the low percent variance explained by this mode for individual displacement time series there. Also, the displacement- and velocity-EOF amplitude functions are not coherent (Table 4). Unlike the near-inertial frequency velocity-EOF amplitude functions, the mode-one displacement-EOF amplitude function is coherent with the rotary wind stress (Table 5). The EOF lags the wind stress by 0.30 days for clockwise rotation and leads by 0.08 days for anticlockwise rotation.

Rotary EOFs were not computed for the near-inertial frequency band using the cross-shelf data set since in that band coherence between currents measured at different across-shelf locations was generally not significant.

7. Diurnal frequency band

a. Vertical EOFs

The clockwise 1_- rotary velocity EOF calculated from the vertical data set for the diurnal frequency band centered at $|f| = 0.98$ cpd, has a rapid increase in amplitude above 15 m (Fig. 7). The surface intensification is associated with a 180° phase change near 15 m. The phase and amplitude below 15 m are nearly constant. The 1_- EOF accounts for 90% of the clockwise variance. It is also highly coherent with the wind stress (0.90 coherence squared) and lags the wind stress by 0.17 days.

The EOF amplitudes for clockwise and anticlockwise rotation are comparable below 15 m. The 1_+ EOF phase and amplitude for anticlockwise rotation indicate a depth-independent structure below 15 m. The 1_+ EOF amplitude function is also coherent with the wind stress (0.66 coherence squared). Above 10 m, the clockwise EOF amplitude is larger than the anticlockwise EOF amplitude. This may be related to the fact that at the diurnal frequency the wind stress has more energy for clockwise than anticlockwise rotation (Fig. 2). Also, in time-dependent Ekman layer theory the amplitude of the complex velocity response to wind forcing with equal magnitudes for both rotations is greater for clockwise than for anticlockwise rotation (Gonella, 1972).

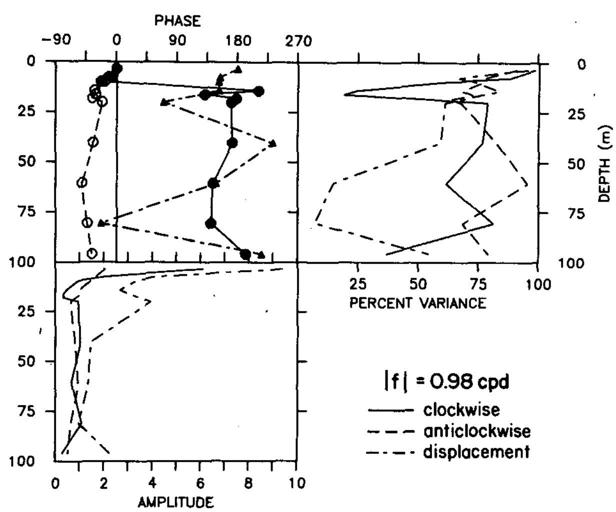

FIG. 7. Rotary first-mode velocity- and displacement-EOF phase (top), amplitude (bottom) and percent variance explained (upper right) as functions of depth (m) for the diurnal frequency band (0.98 cpd) and the vertical data set. Notation is the same as for Fig. 4. The velocity and displacement EOF amplitudes are in cm s^{-1} and 10^{-1} m, respectively.

The rotary ellipse orientation for mode one is across the shelf. The rotary coefficient indicates clockwise rotation. The EOF amplitudes and phases for modes 1_+ and 1_-, and the ellipse-axis orientation and stability squared, indicate cross-shelf rectilinear flow below 15 m and nearly circular clockwise rotation above 15 m. This structure, together with the mode 1_- surface intensification and high coherence with the wind stress, indicate a wind-forced surface transport with a compensating cross-shelf transport below. The above is qualitatively consistent with a two-dimensional mass balance normal to the coast.

The mode-one displacement-EOF amplitude function (Fig. 7) is highly coherent (0.88 coherence squared) with the wind stress for both rotations. The phase between the displacement-EOF amplitude function and the wind is −57° for clockwise rotation and −107° for anticlockwise rotation (Table 5). The displacement- and velocity-EOF amplitude functions are also coherent. This coherence, the coherence of the wind stress and the displacement-EOF amplitude function, and the surface intensification in displacement-EOF amplitude may indicate wind-forced advection of horizontal temperature gradients.

b. *Cross-shelf EOFs*

The mode 1_- EOF amplitude and phase calculated from the cross-shelf data set are plotted in Fig. 8. Mode 1_- with 57% of the total clockwise variance is fairly depth-independent at Forsythia and Carnation. The magnitudes of the EOF phase differences are generally less than 90°. At Forsythia the velocity vectors have slight rotation with depth. At Carnation, the phase differences are somewhat larger, with the velocity vector at C96 rotated 90° relative to the other Carnation velocities. The four time series at E20, E120, C60 and A20 have only a small percentage of their total variance explained by mode 1_-. Most of the variance for E20, E120, C60 and A20 is in modes two, four, three and two, respectively.

The amplitude of the mode 1_+ EOF, with 84% of the total anticlockwise variance, is nearly independent of depth and offshore distance. The same is generally true for phase with the largest differences occurring at the nearshore locations C20, A20 and A40. The percent of the variance accounted for by the 1_+ EOF for each time series is high with the smallest value being 59% at C20.

The rotary statistics for the diurnal frequency band are indicative of an anticlockwise rotating velocity vector with alongshore ellipse orientation. The relatively small rotary coefficient (+0.26) and the appreciable stability squared (0.51) indicate some tendency toward rectilinear flow along 69°, nearly alongshore. The mode-one EOF amplitude functions for both rotations are significantly coherent with the wind stress. The mode-one EOF leads the wind stress for clockwise and anticlockwise rotation by 0.3 and 0.4 days, respectively. The relation to the wind stress is similar to that found from the vertical data set and evidently reflects the existence of a wind-forced surface layer with compensating cross-shelf transport below.

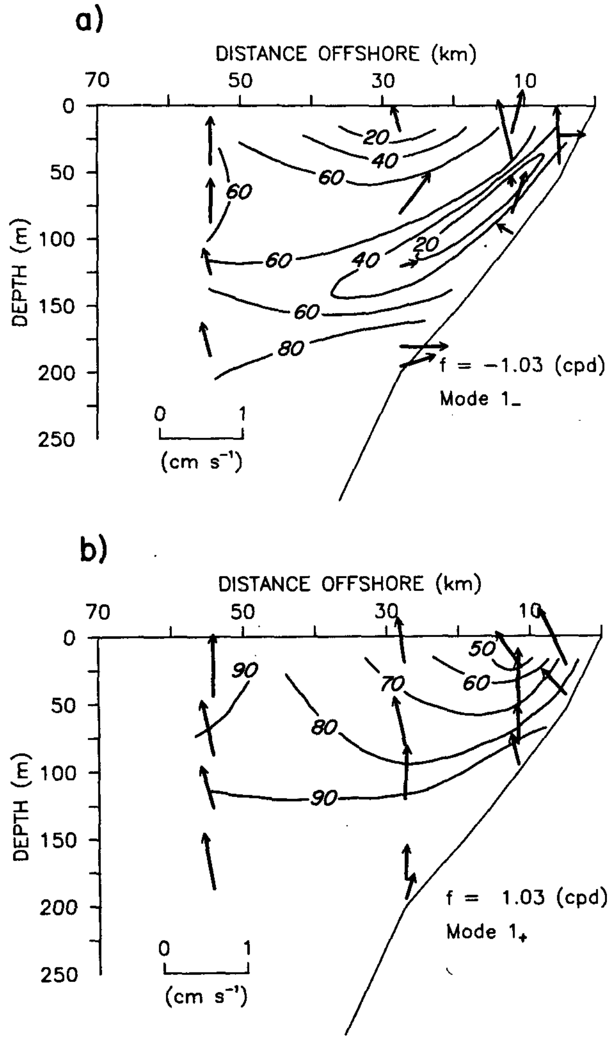

FIG. 8. As in Fig. 5 but at the diurnal frequency (1.03 cpd) for the cross-shelf data set.

8. Low frequencies

a. *Vertical EOFs*

The first-mode EOF amplitude and phase calculated from the vertical data set are plotted as functions of depth and frequency in Fig. 9. The upper 20 m were contoured separately since the instrument separation is much smaller above 20 m depth.

The EOF amplitude has two maxima: a subsurface maximum of 7 cm s^{-1} at 60 m and −0.056 cpd, and a surface maximum of 8 cm s^{-1} at 0.056 cpd. The amplitude is nearly constant with depth at frequencies higher than 0.056 cpd. Below 20 m, the EOFs for

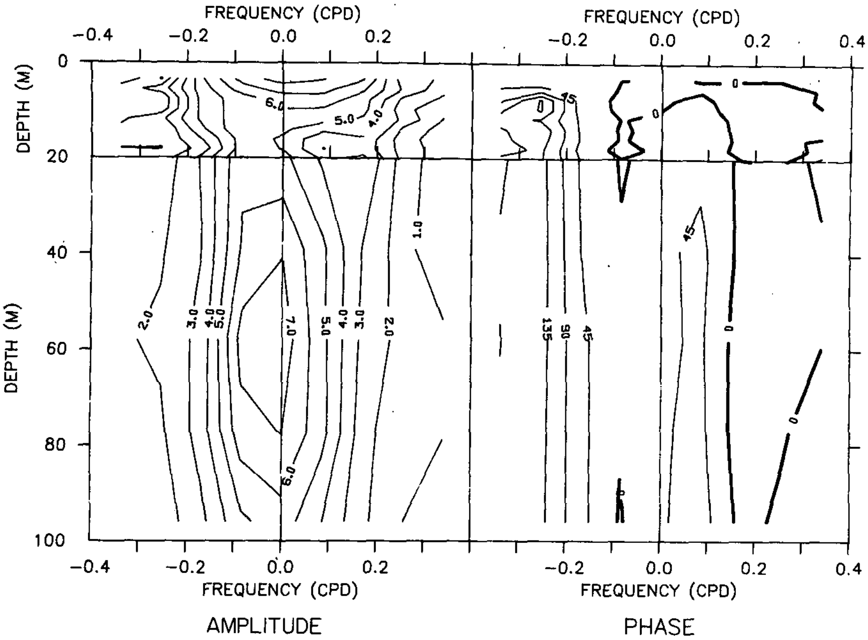

FIG. 9. Rotary first-mode velocity-EOF amplitude (left) and phase (right) as functions of depth (m) and frequency (cpd) for the vertical data set. The EOF amplitude contours are isotachs (1 cm s^{-1} contour interval) and the EOF phase contours are lines of constant phase (45° contour interval).

clockwise rotation have larger amplitudes. This agrees with the general clockwise rotation found by Kundu and Allen (1976) in hodograph plots of a complex-time-domain EOF calculated for a similar cross-shelf data set from the CUE-II observations.

The EOF phase is fairly constant in the vertical at each frequency. The phase is most variable in the surface layer. Surface-to-bottom phase differences are typically 40° or less. EOF phase and amplitude are consistent with current ellipses that are highly eccentric, oriented alongshore and nearly depth-independent in amplitude. Since the low-frequency velocity fluctuations are nearly rectilinear, rotary EOF analysis may not be the optimum investigative tool for this frequency range.

b. Cross-shelf EOFs

The EOF amplitude and phase calculated from the cross-shelf data set are depicted by vectors in Fig. 10 for a frequency band centered at 0.25 cpd. The structures for both 1_- and 1_+ are depth-independent with decreasing amplitude offshore. The rotary coefficient $C_r = -0.27$ and stability squared $|E|^2 = 0.77$ indicate slight clockwise rotation consistent with the results from the vertical data set, but the flow is nearly rectilinear. The axis orientation is $-77°$, nearly alongshore.

From analysis of the same CUE-II data, Hsieh (1982) claims to find that the cross-shelf structure of the horizontal velocity field is dominated by the second barotropic shelf-wave mode. The zero-crossings of the alongshore velocity in the cross-shelf modes of shelf waves are indicated by changes in the sign of the rotary coefficient C_r (Hsieh, 1982). Rotary EOFs will separate the regions of negative and positive C_r into clockwise and anticlockwise modes, respectively. Thus, the presence of a zero-crossing should be accompanied by a change in the cross-shelf direction of the relative amplitudes of the clockwise and anticlockwise EOFs, i.e., $A_j^1(f') > A_j^1(-f')$ should change to $A_k^1(f') < A_k^1(-f')$ across a zero-crossing of the alongshore velocity. No indication of a zero-crossing is found here, in agreement with results from the cross-shelf complex time-domain EOFs of Kundu and Allen (1976). This, of course, gives no direct evidence for the presence of cross-shelf coastal-trapped wave modes higher than the first.

9. Summary

Current meter data from the CUE-II experiment off Oregon have been analyzed using rotary empirical orthogonal functions (EOFs). The EOF amplitude functions may be calculated from the eigenvectors of the cross-spectral matrix and the autospectra (3.8) and may be used to calculate directly the cross-spectra with other series, e.g., wind stress. The fraction of variance explained by EOF mode i for the series at position j is the coherence squared between EOF amplitude function i and series j (3.14). Likewise, the EOF phase of mode i at position j may be interpreted as the phase between EOF amplitude function i and series j (3.15).

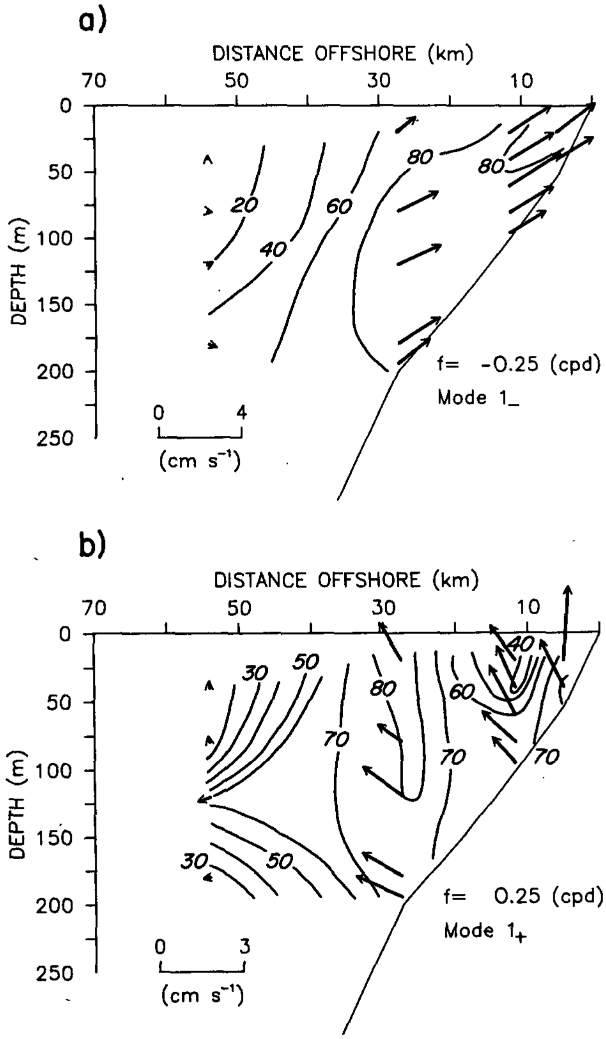

FIG. 10. As in Fig. 5 but at 0.25 cpd for the cross-shelf data set. Note difference in velocity scale.

Rotary EOF analysis was performed on the vertical and cross-shelf data sets for the semidiurnal, near-inertial and diurnal frequency bands and for frequencies below 0.3 cpd. For the semidiurnal frequency band, the clockwise rotary velocity EOFs have a strong baroclinic structure (Figs. 4 and 5) with nodes in the vertical typically at 0.4 times the water depth. The phase relations between displacement and velocity imply onshore propagation with a cross-shelf wavelength of 40 km. The anticlockwise velocity EOF is nearly depth-independent and the amplitude function is coherent with the clockwise velocity-EOF amplitude function. This is consistent with the M_2 barotropic tide forcing a clockwise rotating M_2 baroclinic tide.

For the near-inertial frequency band, results from the EOF analysis with the vertical data set (Fig. 6) show that most of the variance is in the clockwise EOF as expected when near-inertial waves are present. The velocity- and displacement-EOF amplitude functions are not coherent with the wind stress or with each other. The depth dependence of the phase for the clockwise velocity EOF is linear with a slope that corresponds to an upward propagation of phase at 0.14 cm s^{-1}. This compares favorably with results of Kundu (1976) from the analysis of the same velocity data using a different method.

For the diurnal frequency band, the velocity EOFs are depth-independent below 10 m for clockwise and anticlockwise rotation (Fig. 7). Above 10 m, there is a 180° phase shift and a rapid increase in amplitude for clockwise rotation. The velocity-EOF amplitude functions are highly coherent with each other and with the wind stress. This evidently corresponds to wind forcing at the diurnal frequency of surface layer motion with a compensating transport in the cross-shelf direction below.

In previous studies of oceanographic data, rotary spectral and rotary cross-spectral calculations have proven useful for the analysis of two-dimensional velocity time series. Likewise, computations of single-sided frequency-domain EOFs have been helpful in the cross-spectral analysis of scalar time series. These two techniques are combined here and a formalism for the construction of rotary EOFs for a set of complex time series is developed. Rotary EOF decomposition has the inherent advantages of both rotary spectra and of frequency-domain EOFs, i.e., it is insensitive to coordinate orientation and it compactly represents information from the entire cross-spectral matrix. Rotary EOFs naturally separate clockwise and anticlockwise rotating motions. For the near-inertial frequency band, the anticlockwise rotating "noise" is automatically removed from the clockwise rotating "signal". The upward phase propagation of near-inertial internal waves is clearly extracted here by rotary EOF analysis. For the semidiurnal frequency band, we found that baroclinic and barotropic structures are separable by direction of rotation. The calculation of cross-spectra between the EOF amplitude functions and other series is readily accomplished by the method described in Section 3 and can provide additional physical information. For example, in the diurnal frequency band the high coherences of the rotary velocity-EOF amplitude functions with the wind stress give strong evidence for wind forcing of velocity structures that are coherent in depth and across the shelf. Based on these positive results, it appears that rotary empirical orthogonal function decomposition should provide another useful tool for the analysis of oceanographic data.

Acknowledgments. This research was supported for both investigators by the Oceanography Section of the National Science Foundation under Grant OCE-8026131 ("SuperCODE") and also for J. S. Allen by National Science Foundation Grant OCE-8014939 (CODE: Coastal Ocean Dynamics Experiment). We thank Drs. R. L. Smith and D. Halpern for providing current, temperature and wind measurements from CUE-II. We also thank Drs. M. Levine and J. Richman for helpful discussions and comments.

REFERENCES

Battisti, D. S., and A. J. Clarke, 1982: Estimation of nearshore tidal currents on nonsmooth continental shelves. *J. Geophys. Res.*, **87**, 7873–7878.

Davis, R. E., R. deSzoeke and P. Niiler, 1981: Variability in the upper ocean during MILE. Part II: Modeling the mixed layer response. *Deep-Sea Res.*, **28A**, 1453–1475.

Denbo, D. W., 1983: On forced currents over a continental margin: Theory and analysis. Ph.D. thesis, Oregon State University.

Gonella, J., 1972: A rotary-component method for analysing meteorological and oceanographic vector time series. *Deep-Sea Res.*, **19**, 833–846.

Gordon, R. L., 1978: Internal wave climate near the coast of northwest Africa during JOINT-I. *Deep-Sea Res.*, **25**, 625–643.

Halliwell, G. R., and C. N. K. Mooers, 1983: Meanders of the Gulf Stream downstream from Cape Hatteras, 1975–1978. *J. Phys. Oceanogr.*, **13**, 1275–1292.

Halpern, D., 1976a: Structure of a coastal upwelling event observed off Oregon during July 1973. *Deep-Sea Res.*, **23**, 495–508.

——, 1976b: Measurements of near-surface wind stress over an upwelling region near the Oregon coast. *J. Phys. Oceanogr.*, **6**, 108–112.

Hogg, N., 1981: Topographic waves along 70°W on the continental rise. *J. Mar. Res.*, **39**, 627–649.

Hsieh, W. M., 1982: On the detection of continental shelf waves. *J. Phys. Oceanogr.*, **12**, 414–427.

Kundu, P. K., 1976: An analysis of inertial oscillations observed near Oregon coast. *J. Phys. Oceanogr.*, **6**, 879–893.

——, and J. S. Allen, 1976: Some three-dimensional characteristics of low-frequency current fluctuations near the Oregon coast. *J. Phys. Oceanogr.*, **6**, 181–199.

Mooers, C. N. K., 1973: A technique for the cross spectrum analysis of pairs of complex-valued time series, with emphasis on properties of polarized components and rotational invariants. *Deep-Sea Res.*, **20**, 1129–1141.

Müller, P., D. J. Olbers and J. Willebrand, 1978: The Iwex spectrum. *J. Geophys. Res.*, **83**, 479–800.

Overland, J. E., and R. W. Preisendorfer, 1982: A significance test for principal components applied to a cyclone climatology. *Mon. Wea. Rev.*, **110**, 1–4.

Pollard, R. T., 1970: On the generation by winds of inertial waves in the ocean. *Deep-Sea Res.*, **17**, 795–812.

Torgrimson, G. M., and B. M. Hickey, 1979: Barotropic and baroclinic tides over the continental slope and shelf off Oregon. *J. Phys. Oceanogr.*, **9**, 945–961.

Wallace, J. M., and R. E. Dickinson, 1972: Empirical orthogonal representation of time series in the frequency domain. Part I: Theoretical considerations. *J. Appl. Meteor.*, **11**, 887–892.

Wang, D-P., and C. N. K. Mooers, 1977: Long coastal trapped waves off the west coast of the United States, summer 1973. *J. Phys. Oceanogr.*, **7**, 856–864.

Weller, R. A., 1982: The relation of near-inertial motions observed in the mixed layer during JASIN (1978) experiment to the local wind stress and to the quasi-geostrophic flow field. *J. Phys. Oceanogr.*, **12**, 1122–1136.